Singlet fission as a polarized spin generator for biological nuclear hyperpolarization

Yusuke Kawashima,[1†] Tomoyuki Hamachi,[1†] Akio Yamauchi,[1] Koki Nishimura,[1] Yuma Nakashima,[1] Saiya Fujiwara,[1] Nobuo Kimizuka,[1,2] Tomohiro Ryu,[3] Tetsu Tamura,[3] Masaki Saigo,[3] Ken Onda,[3] Shunsuke Sato,[4] Yasuhiro Kobori,[5,6] Kenichiro Tateishi,[7,8] Tomohiro Uesaka,[7,8] Go Watanabe,[4,9]* Kiyoshi Miyata,[3]* and Nobuhiro Yanai.[1,2,10]*

[1] Department of Applied Chemistry, Graduate School of Engineering, [2]Center for Molecular Systems (CMS), and [3]Department of Chemistry, Graduate School of Science, Kyushu University, 744 Moto-oka, Nishi-ku, Fukuoka 819-0395, Japan.

[4] Department of Physics, School of Science, Kitasato University, Sagamihara, Kanagawa 252-0373, Japan.

[5] Molecular Photoscience Research Center and [6]Department of Chemistry, Graduate School of Science, Kobe University, 1-1, Rokkodai-cho, Nada-ku, Kobe 657-8501, Japan.

[7] Cluster for Pioneering Research, RIKEN, and [8]RIKEN Nishina Center for Accelerator-Based Science, 2-1 Hirosawa, Wako, Saitama 351-0198, Japan

[9] Kanagawa Institute of Industrial Science and Technology (KISTEC), 705-1 Shimoizumi, Ebina, Kanagawa 243-0435, Japan.

[10] PRESTO, JST, Honcho 4-1-8, Kawaguchi, Saitama 332-0012, Japan.

*Corresponding author. Email: go0325@kitasato-u.ac.jp (G.W.); kmiyata@chem.kyushu-univ.jp (K.M.); yanai@mail.cstm.kyushu-u.ac.jp (N.Y.)

[†]These authors contributed equally to this work.

Abstract: Singlet fission (SF), converting a singlet excited state into a spin-correlated triplet-pair state, is the sole way to generate a spin quintet state in organic materials. Although its application to photovoltaics as an exciton multiplier has been extensively studied, use of its unique spin degree of freedom is largely unexplored. Here, we demonstrate that the spin polarization of the quintet multiexcitons generated by SF improves the sensitivity of biological magnetic resonance through dynamic nuclear polarization (DNP). We form supramolecular assemblies of a few pentacene chromophores and use SF-born quintet spins to achieve DNP of water-glycerol, the most basic biological matrix, at lower microwave intensities than for conventional triplet-based DNP. Our demonstration opens a new use of SF as a "polarized spin generator" in bio-quantum technology.

Main text: Photo-excited states of organic assemblies have brought a number of unique opportunities to optoelectronics, taking advantage of the dual nature of singlet and triplet molecular excitons [1]. In particular, singlet fission (SF) [2-12], which generates two triplet excitons from one singlet exciton, shows unique functions in terms of electron and spin degrees of freedom. SF is a multiexciton generation process that can potentially surpass the theoretical limit of a single-junction solar cell if the split excitons are harvested as free electrons and holes [5]. Its unique electron degree of freedom has attracted much attention and has been studied intensively for decades.

The basic SF process is as follows: the singlet exciton S_1 undergoes a spin-allowed ultrafast transition to a triplet-pair state with overall-singlet multiplicity, ^{1}(TT), followed by an intersystem crossing (ISC) to the highest spin multiplicity state, a *quintet* triplet-pair ^{5}(TT). When the molecular assembly is larger than two molecules, the triplet-pair states may dissociate into two free triplets [9, 13-16]. Note that the multiexcitonic nature offers a unique opportunity to construct quintet multiplicity owing to the presence of four half-filled orbitals. SF provides the sole method to create spin quintet states in organic molecular systems without heavy metals. However, how to use this unique quintet state has not been fully demonstrated.

In the second quantum revolution, we explore the unique spin degree of freedom of SF for quantum technologies [17, 18]. It has been revealed that the $|^5(\mathrm{TT})_0\rangle$ spin sublevel with a magnetic quantum number $m_s = 0$ can be selectively populated among five quintet sublevels because the state immediately after photoexcitation is a spinless singlet state, and the transitions occur by preserving its total spin [13-16]. To date, the spin aspect of SF has only been used to explain the microscopic mechanisms of SF. Because organic spin materials have advantages with their extremely small size, down to nanometers, and excellent bio-compatibility, it is worthwhile to research applications of the unique quintet state in quantum information science (QIS) and quantum biotechnologies [17, 18].

Dynamic nuclear polarization (DNP) of biomolecules is one of the fields where polarized electron spins can play a pivotal role [19-26]. Nuclear magnetic resonance (NMR) and magnetic resonance imaging (MRI) are indispensable analytical techniques in modern life science and medicine, but their critically low sensitivity limits their applications. Many trials of MRI diagnosis of cancer have been conducted by transferring the polarization of radical electron spins, which are in thermal equilibrium at cryogenic temperatures near 1 K, to the nuclear spins of bioprobes, and then dissolving them and administering them to the human body [27]. However, the equipment is inevitably expensive and complicated because it requires cryogenic temperatures. Thus there is a strong need to develop DNP using polarized electron spins generated at higher

temperatures. The triplet excited state generated by spin-selective ISC from a photoexcited singlet has been used as a polarized spin source [28], but the polarization ratio of the triplet is usually far less than 100% [29]. However, SF has the potential to offer the ultimate polarization source because it can selectively populate the $|^5(TT)_0\rangle$ spin sublevel through its intrinsic mechanism, and it occurs in nanoseconds with a quantum yield of up to 200% [2].

This study demonstrates the first application of an SF-born polarized quintet state in biological DNP. Various small biomolecules and proteins can be hyperpolarized by dispersing them in an amorphous water-glycerol glass [19]. The key to successful DNP in a bio-oriented water-glycerol environment is to regulate the balance between aggregation and dispersion of SF molecular assembly; more than two molecules are needed for SF, but aggregation that is too large hampers the polarization transfer from the SF-generated electron spins to the nuclear spins. In essence, creating robust dimer aggregates would best achieve both efficient SF and polarization transfer to the water-glycerol and eventually to dispersed biomolecules. We focus on a pentacene derivative, the most representative chromophore exhibiting SF [8]. We succeed in constructing discrete assemblies of pentacene moieties in water-glycerol using two distinct strategies: supramolecular assembly of an amphiphilic pentacene derivative and complexation with cyclodextrin (CD) [30]. The combination of ultrafast pump-probe transient absorption spectroscopy (TAS) and time-resolved electron spin resonance (ESR) measurements reveals that either pentacene assembly undergoes SF and populates the specific quintet sublevel. We succeed in DNP of water-glycerol by transferring the polarization from quintet electron spins to nuclear spins upon microwave irradiation to satisfy the Hartmann-Hahn condition (Fig. 1B, 1C). In addition, we show that quintets with higher Rabi frequencies can cause DNP at lower microwave intensities than a conventional triplet [17], demonstrating the potential of SF in quantum biotechnology.

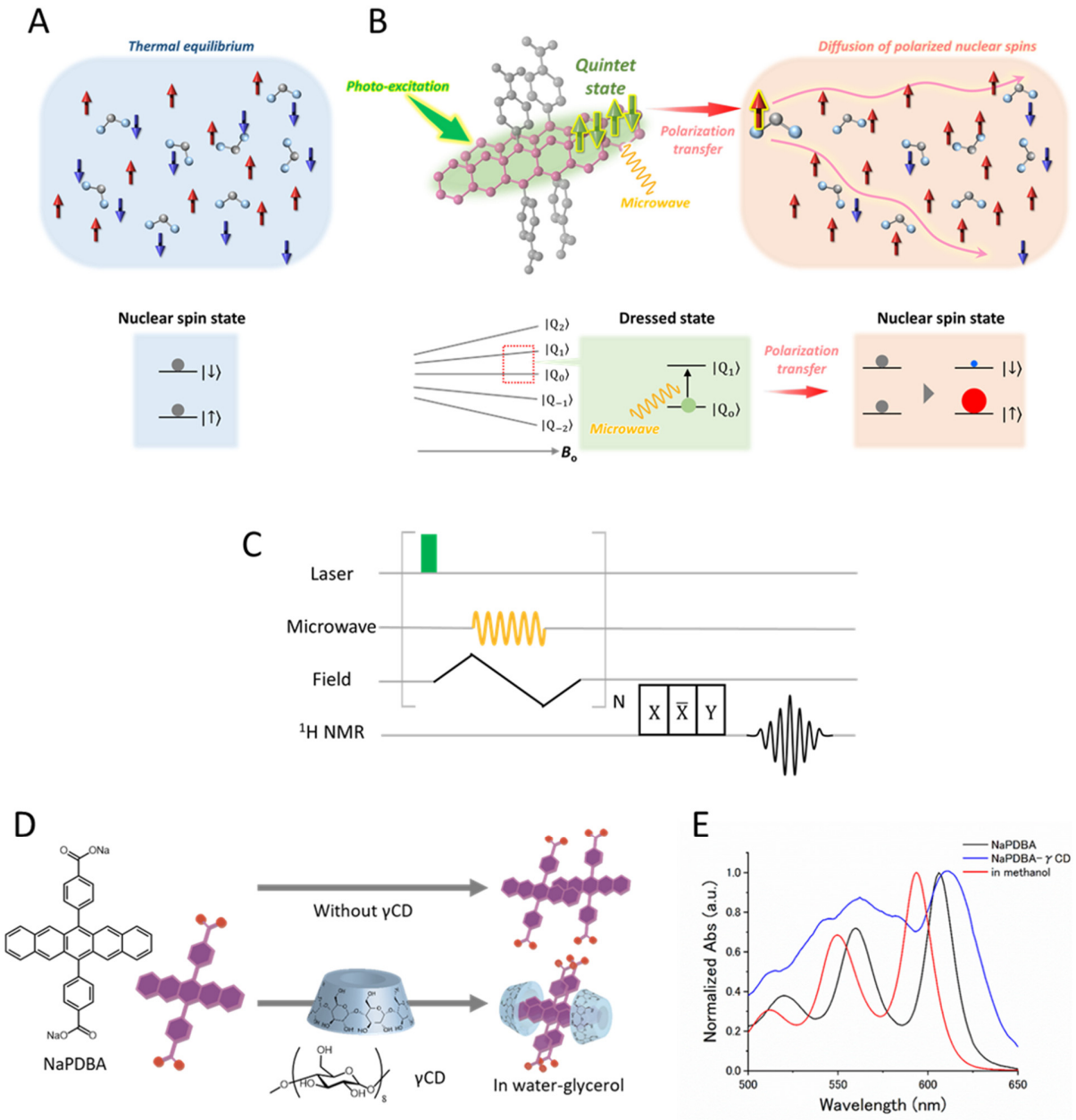

Fig. 1. Schematic illustration of DNP using SF-born quintet electron polarization. (A) Nuclear spins in the thermal equilibrium state. (B) Polarization transfer from electron spins in the quintet state generated by photo-induced SF to nuclear spins and the subsequent diffusion of hyperpolarized nuclear spins. (C) Pulse sequence of quintet/triplet-DNP. (D) Molecular structures of NaPDBA and γ-cyclodextrin (γCD) and supramolecular assembly of only NaPDBA and the NaPDBA-γCD inclusion complex. (E) Absorption spectra of NaPDBA in water-glycerol at 143 K (black), NaPDBA-γCD in water-glycerol (1:1) at 143 K (blue), and NaPDBA in methanol at room temperature (red). The concentrations of NaPDBA and γCD were 1 mM and 5 mM, respectively.

To construct supramolecular assemblies showing SF, we used our previously developed amphiphilic sodium 4,4′-(pentacene-6,13-diyl)dibenzoate (NaPDBA, Fig. 1D): a hydrophobic pentacene modified with hydrophilic carboxyl groups. We molecularly dispersed 1-mM NaPDBA in methanol and obtained an absorption peak at 593.5 nm. In water-glycerol, the absorption peak was clearly red-shifted to 604 nm, suggesting the formation of supramolecular assemblies (Fig. 1E). We adjusted the mixing ratio of water and glycerol and used a 1:1 mixture by volume because it maintains the glassy state in the DNP-relevant condition, i.e., low temperature under laser irradiation. Molecular dynamics (MD) simulation was performed for an initial structure of 20 molecules of NaPDBA in close proximity to each other in water-glycerol. The simulation showed that the structure split into multiple dimers and a few monomers (Fig. 2A). In the dimers, the pentacene units were oriented in parallel to form a slipped-stack with an average distance of 0.6 nm between the centers of mass of the dimers (Fig. 2B). The formation of small dimeric structures agrees well with the fact that dynamic light scattering (DLS) measurements of NaPDBA in water-glycerol did not show any significant scattering intensity derived from large aggregates. However, DLS measurements showed that NaPDBA forms larger structures in pure water without glycerol (Fig. S1). MD simulations also confirmed the formation of stable NaPDBA multimers in water (Fig. S2). The addition of glycerol may have weakened the hydrophobic interactions between NaPDBA monomers and prevented the formation of larger aggregates, leading to the formation of NaPDBA dimers [31].

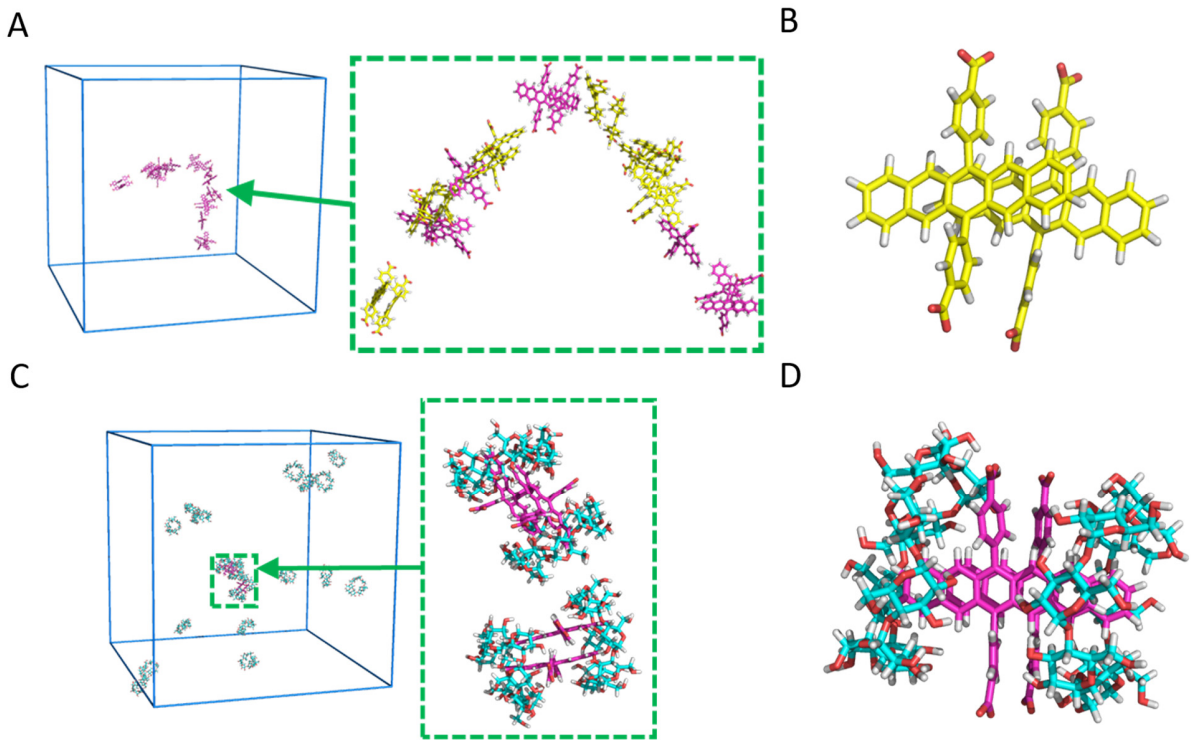

Fig. 2. MD simulation of the supramolecular assemblies. (A,B) MD simulation snapshots of NaPDBA ([NaPDBA] = 1 mM) in water-glycerol (1:1) at 300 K. Parallel oriented dimers are shown in yellow. (C,D) MD simulation snapshots of NaPDBA and γCD ([NaPDBA] = 1 mM, [γCD] = 5 mM) in water-glycerol (1:1) at 243 K.

To systematically change the assembly structure and excitonic interaction between pentacene moieties while using the same NaPDBA molecule, we added β-cyclodextrin (βCD) and γ-cyclodextrin (γCD) to NaPDBA in water-glycerol. βCD and γCD are cyclic oligosaccharides with seven and eight glucose subunits, respectively, and can host various hydrophobic compounds within their hydrophobic interiors. The addition of γCD did not change the absorption spectrum of NaPDBA at room temperature with an absorption peak at 604 nm (Fig. S4). Notably, the absorption peak of NaPDBA was further red-shifted to 612 nm and broadened by cooling to 143 K after inclusion was allowed to fully progress by letting the solution stand at 243 K in the presence of γCD (Fig. 1E, S4). This suggests that the inter-pentacene excitonic interaction was enhanced by the formation of the inclusion complex between NaPDBA and γCD at low temperature. NMR studies of NaPDBA and γCD suggested that two molecules of γCD encapsulate a NaPDBA dimer, which is reasonable considering the large inner diameter of γCD and the observed strong excitonic interaction between pentacene moieties in the NaPDBA-γCD inclusion complex (see Supporting Information for details). In the MD simulation, the 2:2 inclusion complex of NaPDBA-γCD was stable in water-glycerol at 243 K (Fig. 2C, D). Note that the inclusion complexes of NaPDBA-γCD were unstable at room temperature in water-glycerol (Fig. S11), which is consistent with the experimental results for complexation only by cooling (Fig. S4). The inclusion of the NaPDBA monomer by two βCD molecules was suggested by the absorption spectra, NMR measurements, and MD simulations (see Supporting Information for details). This 1:2 inclusion complex of NaPDBA-βCD without SF was used for comparison.

To investigate the SF properties of these systems, we conducted femtosecond and nanosecond pump-probe TAS (fs- and ns-TAS) measurements in water-glycerol glass at 143 K, which is relevant to ESR and DNP measurements. Prior to the TAS measurements, the water-glycerol solutions of NaPDBA and NaPDBA-βCD were quenched and vitrified in liquid nitrogen after complexation at 243 K. The excitation wavelength was set at the lowest absorption edge (600-635 nm) to minimize the excess photoexcitation energy. Figure 3 shows a thorough comparison of fs-TAS measurements of the systems and the corresponding results of global analyses. The bare NaPDBA aggregates showed broad transient absorption with a peak at 430-450 nm just after photoexcitation (Fig. 3A-C), which can be assigned to the transition from the S_1 excited state (S_1-S_n transition). For pentacene-based systems, the presence of SF can be estimated from the ultrafast growth of transient absorption around 510-520 nm typically assigned to the T_1-T_n transition of a pentacene skeleton [8]. As the peak around 450-460 nm decreased in several picoseconds, the TA around 510-520 nm became dominant. This allowed us to confirm the ultrafast generation of T_1 through SF of NaPDBA aggregates. To quantify the ultrafast SF process, we globally analyzed the observed fs-TAS assuming a sequential model with two components (Fig. 3C-E). The first component was converted to the second component with a time constant of 2.65±0.01 ps, followed by negligible decay (> 1 ns) in the current time window. Note that the first and second components of the evolution-associated spectra (EAS) can reasonably be assigned from their shapes to the spectra from S_1 and T_1, respectively. Because the transition timescale is much quicker than that of typical ISC, we concluded that the transition of the first step of SF, $S_1 \rightarrow {}^1(TT)$, in the NaPDBA aggregates occurs with a time constant of 2.65 ps. We also observed an increase in T_1-T_n absorption for ~7 ns in ns-TAS, which was assigned to the ISC of monomolecularly dispersed NaPDBA (Fig. S13). This implies that the system consisted of a mixture of monomeric and dimeric NaPDBA, consistent with the MD simulation.

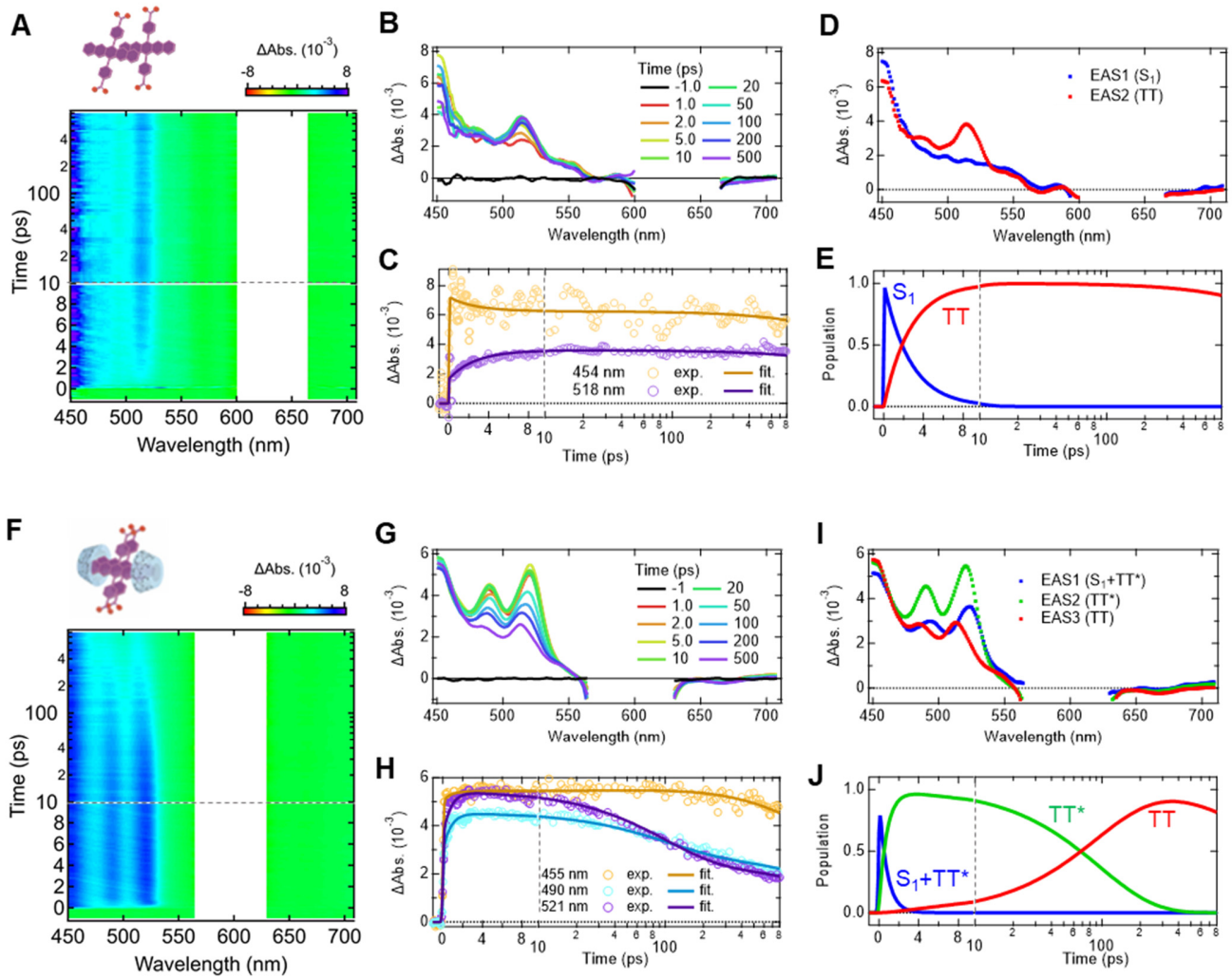

Fig. 3. fs-TAS measurements of the supramolecular assemblies. Overview of fs-TAS analysis of (A-E) NaPDBA and (F-J) NaPDBA-γCD in water-glycerol (1:1) at 143 K ([NaPDBA] = 1 mM, [γCD] = 5 mM). (A, F) Pseudo-2D plots of experimentally observed fs-TAS (excitation: 635 nm for NaPDBA and 600 nm for NaPDBA-γCD), (B, G) spectral evolution of the TAS, and (C, H) temporal change of transient absorption at selected wavelengths and fitting curves from global analysis. (D, I) Evolution-associated spectra and (E, J) corresponding concentration kinetics obtained from global analysis based on sequential models.

For the NaPDBA-γCD complex, the TAS around 510-520 nm emerged rapidly after photoexcitation concurrently with the broad absorption around 450-500 nm (Fig. 3F-H). The spectral shape of the initial TA was also different from that observed for the bare NaPDBA aggregates. The complicated behavior of the TAS can be globally fitted with a three-component sequential model (Fig. 3H-J). Though the first and second EAS components look unique, the third resembles that of the bare NaPDBA aggregates. Because the complexation with γCD results in the tightly packed dimer, strong electronic coupling between the adjacent pentacene moieties likely forms a heavily mixed electronic excited state of S_1 and the triplet pair states (S_1+TT). After formation of the mixed-excited state, dephasing into a pure TT state (TT*) occurs. The

TT* state relaxes to form a geometrically relaxed triplet pair state (TT), which competes with deactivation to S_0 as reflected in the decreased absorption in the third EAS component. Similar behaviors were observed in NaPDBA systems in water at room temperature (Fig. S14). In stark contrast, negligible SF was observed in the βCD complex (Fig. S15), consistent with the monomolecularly dispersed picture in which the inter-chromophore interactions are significantly weakened by the complexation of a single NaPDBA molecule with two βCD molecules (Fig. S9).

Overall, we concluded that sub-ns T_1 generation due to SF occurs in the bare NaPDBA dimers and NaPDBA-γCD complex, while the NaPDBA-βCD complex does not show significant SF. Note that ns-TAS measurements of the NaPDBA and NaPDBA-βCD systems also showed slower T_1 generation due to ISC from S_1 to T_1 (Fig. S13). Additionally, fs-TAS and ns-TAS showed subtle excitation wavelength dependences (details are in Fig. S16). This suggested that both aggregated and isolated NaPDBA coexisted in the water-glycerol glass systems, and both SF-derived and ISC-derived triplets were generated with light irradiation.

Having concrete evidence of SF, we performed time-resolved ESR measurements to evaluate the transient electron spin polarization of these supramolecular assemblies in water-glycerol glass. The samples were prepared in the same way as for the TAS measurements, except that glass capillaries were used. As expected from the SF found in the NaPDBA-only assemblies and the NaPDBA-γCD complex, a signal derived from the quintet was observed at a position where the peak width was about one-third that of the triplet (Fig. 4) [13-16]. These ESR spectra could be fitted as a quintet-triplet superposition. The spectra were simulated using a geometric fluctuation model of the quintet multiexcitions between two strongly coupled TT conformations (TT_1 and TT_2) with different orientations and *J*-couplings following a previous report [16]. We assumed the conformations of the TT_1 and TT_2 states to be parallel and slightly off parallel, respectively. Interestingly, the pentacene moieties were found to be oriented parallel to each other to form the ^{5}(TT) dimer, which agrees well with the MD simulations. The fitting parameters are summarized in Tables S1 and S2. The $|^5(TT)_2\rangle$, $|^5(TT)_0\rangle$, and $|^5(TT)_{-2}\rangle$ sublevels were found to be selectively populated with S_1 and ^{1}(TT) states in both systems when the external magnetic field (B_0) was applied to in-plane directions of the aromatic planes of the complexes. These field orientations thus dominantly contribute to the $^5(TT)_0 \rightarrow {}^5(TT)_1$ microwave transition in Fig. 4. The isolated triplet is produced by the ISC of a single pentacene unit, which also agrees well with the MD simulation and TAS results. The polarization lifetime of the quintet of NaPDBA aggregates and the NaPDBA-γCD complex were 5.5 and 1.8 μs, respectively (Fig. S17D, F), and was determined by the deactivation of the multiexcitons as observed in the ns-TAS (Fig. S13D). This time constant is sufficient to transfer the polarization to the nuclear spins by microwave irradiation. It is notable that the SF-derived polarization was long enough in the water-glycerol glass, the most important biological DNP matrix. The ESR spectrum of the NaPDBA-βCD complex showed only the ISC-derived triplet signal and no quintet signal (Fig. S17B).

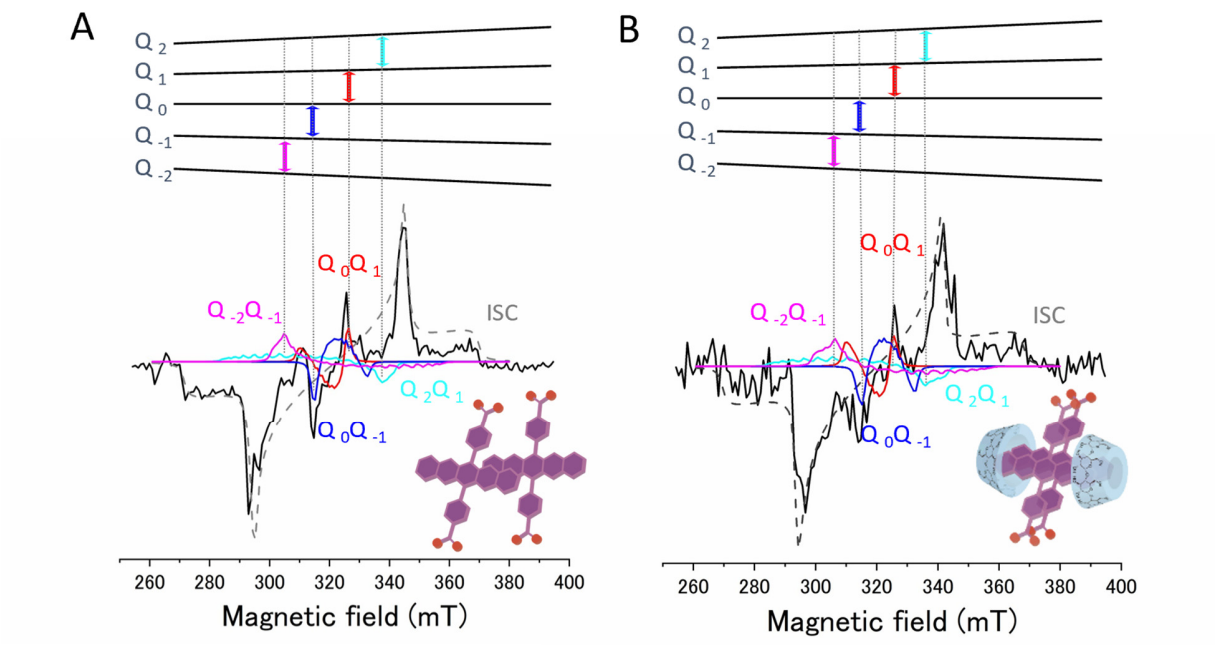

Fig. 4. Time-resolved ESR measurements of the supramolecular assemblies. Time-resolved ESR spectra of (A) NaPDBA and (B) NaPDBA-γCD in water-glycerol (1:1) at 143 K ([NaPDBA] = 1 mM, [γCD] = 5 mM) just after photoexcitation at 527 nm and simulated spectrum. The fitting parameters of the ISC-born triplet and SF-born quintet are summarized in Tables S1 and S2, respectively.

DNP was then performed using the polarized electron spins produced in these supramolecular assemblies. The samples were prepared in a similar way as for the TAS and ESR measurements using a 5-mm ESR tube. To selectively polarize protons of water molecules and extend the spin-lattice relaxation time of ^{1}H, we used a solvent mixture of deuterated glycerol, D_2O, and H_2O in the volume ratio 5:4:1. The DNP sequence shown in Fig. 1C was performed with the central magnetic field aligned with the ESR peaks derived from the quintet. Remarkably, an increase in the ^{1}H NMR signal intensity was clearly observed for the NaPDBA-only assemblies and the NaPDBA-γCD complex at a position corresponding to the $^5(TT)_0 \rightarrow {}^5(TT)_1$ ESR peak (Fig. S19A, C). However, this enhancement was not observed in the NaPDBA-βCD complex, which did not show the quintet-derived signal (Fig. S19B). These results indicate that nuclear hyperpolarization of a biological matrix was successfully achieved using SF-derived quintet electron polarization for the first time.

The difference in the obtained ^{1}H polarization enhancement depends on several factors including the generation efficiency and polarization ratio, the polarization lifetime, and the spin-lattice relaxation of the nuclear spins around the polarizing agents. In the NaPDBA-only sample, there was a 20-fold enhancement at the quintet ESR peak (Fig. 5A). A smaller enhancement of 6.5-fold was observed for the NaPDBA-γCD complexes. Because the ESR spectral analysis showed a similar singlet recombination rate constant from the ^{1}(TT) dimer, the lower enhancement factor of the NaPDBA-γCD complex was probably due to the triplet deactivation caused by triplet-triplet annihilation (TTA) between neighboring pentacenes, as observed in ns-TAS. This indicates the importance of proper arrangement and interaction between pentacene

units. Further support for this is that the build-up time was slowed down to the same level as the spin-lattice relaxation time only for the NaPDBA-γCD complex (Fig. S20, S21). This suggests that not enough electron spin polarization was produced for DNP, as shown by the lower ESR signal-to-noise ratio compared with the NaPDBA-only sample, showing that many triplets are deactivated in the strongly interacting pentacene dimer (Fig. S17A,C).

We then checked the dependence of the microwave intensity irradiated during the DNP sequence using the quintet and triplet electron spin polarizations (Fig. 5C). The NMR signal was found to be maximized at a weaker microwave intensity with the quintet than with the triplet. This is because the Rabi frequency of electrons in the quintet state is $\sqrt{3}$ times higher than that in the triplet state [17], and the Hartmann-Hahn condition is accordingly shifted. The lower microwave intensity is the advantage of the quintet over the conventional triplet for DNP applications.

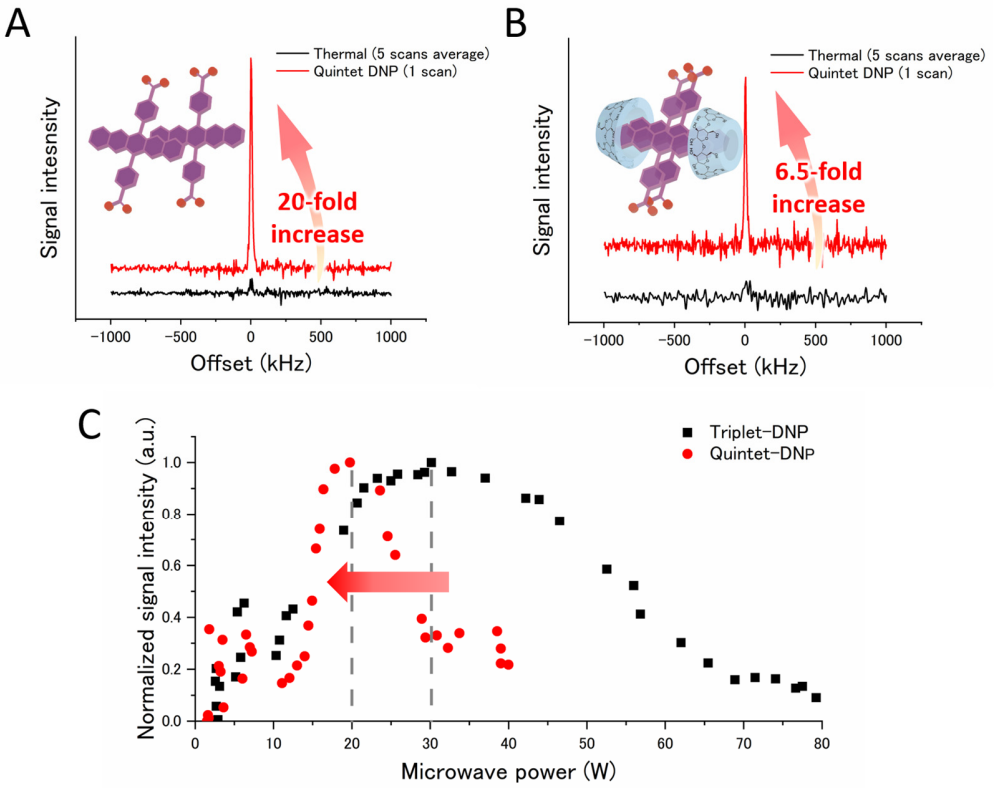

Fig. 5. DNP using SF-born quintet electron spin polarization. ^{1}H-NMR signals under thermal conditions (black lines, 5 scans every 10 min) and after quintet-DNP (red lines, ISE sequence for 5 min, 1 scan) of water-glycerol (glycerol-d_8:D_2O:H_2O = 5:4:1) containing (A) NaPDBA and (B) NaPDBA-γCD at 100 K ([NaPDBA] = 1 mM, [γCD] = 5 mM). The photo-excitation wavelength and frequency were 527 nm and 500 Hz, respectively. DNP was performed by matching the magnetic field to the quintet peaks (26.9 MHz). The microwave power was 20 W, the laser powers were 2.7 W (A) and 1.5 W (B), and the magnetic field sweep width was 10 μs. (C) Microwave power dependence of DNP enhancement. Triplet-DNP was performed at 27.4 MHz (ISE sequence for 10 s and 4 scans with a laser power of 2.7 W and sweep width of 25 μs). Quintet-DNP was performed at 26.9 MHz (ISE sequence for 10 s and 10 scans with a laser power of 2.7 W and sweep width of 10 μs).

In this study, we have demonstrated the potential of SF as a "polarized spin generator" in biological DNP. We have created three supramolecular systems with different interactions between pentacene units using the identical complex of NaPDBA with β/γCD. SF was observed for the NaPDBA-only assemblies and the NaPDBA-γCD complex in water-glycerol glass, where the pentacene skeletons are close to each other. The promising potential of SF as a polarization source was indicated by the selective population of the $|^5(\mathrm{TT})_0\rangle$ sublevel at a particular resonance magnetic field strength. In addition, the quintet-derived polarization allows DNP to be performed at lower microwave intensities than in conventional triplet-DNP. Our findings indicate that the enhancement factor of DNP varies with assembly structure, indicating the direction of further optimizations. Until now, SF has been mainly limited to the field of energy. This study opens a new potential application of SF to quantum biotechnology, and will accelerate the development of quantum sensing and quantum information science based on the unique multiexcitons exhibited by organic chromophores.

References

1. M. A. Baldo, D. F. O'Brien, Y. You, A. Shoustikov, S. Sibley, M. E. Thompson, S. R. Forrest, Highly efficient phosphorescent emission fromorganic electroluminescent devices. *Nature* **395**, 151-154 (1998).
2. J. J. Burdett, A. M. Muller, D. Gosztola, C. J. Bardeen, Excited state dynamics in solid and monomeric tetracene: The roles of superradiance and exciton fission. *J. Chem. Phys.* **133**, 144506 (2010).
3. M. B. Smith, J. Mich, Singlet Fission. *Chem. Rev.* **110**, 6891-6936 (2010).
4. W.-L. Chan, M. Ligges, A. Jailaubekov, L. Kaake, L. Miaja-Avila, X.-Y. Zhu, Observing the Multiexciton State in Singlet Fission and Ensuing Ultrafast Multielectron Transfer. *Science* **334**, 1541-1545 (2011).
5. D. N. Congreve, J. Lee, N. J. Thompson, E. Hontz, S. R. Yost, P. D. Reusswig, M. E. Bahlke, S. Reineke, T. V. Voorhis, M. A. Baldo, External Quantum Efficiency Above 100% in a Singlet-Exciton-Fission–Based Organic Photovoltaic Cell. *Science* **340**, 334-337 (2013).
6. S. W. Eaton, L. E. Shoer, S. D. Karlen, S. M. Dyar, E. A. Margulies, B. S. Veldkamp, C. Ramanan, D. A. Hartzler, S. Savikhin, T. J. Marks, M. R. Wasielewski, Singlet exciton fission in polycrystalline thin films of a slip-stacked perylenediimide. *J. Am. Chem. Soc.* **135**, 14701-14712 (2013).
7. A. J. Musser, M. Al-Hashimi, M. Maiuri, D. Brida, M. Heeney, G. Cerullo, R. H. Friend, J. Clark, Activated singlet exciton fission in a semiconducting polymer. *J. Am. Chem. Soc.* **135**, 12747-12754 (2013).
8. S. N. Sanders, E. Kumarasamy, A. B. Pun, M. T. Trinh, B. Choi, J. Xia, E. J. Taffet, J. Z. Low, J. R. Miller, X. Roy, X. Y. Zhu, M. L. Steigerwald, M. Y. Sfeir, L. M. Campos, Quantitative Intramolecular Singlet Fission in Bipentacenes. *J. Am. Chem. Soc.* **137**, 8965-8972 (2015).
9. G. D. Scholes, Correlated Pair States Formed by Singlet Fission and Exciton-Exciton Annihilation. *J. Phys. Chem. A* **119**, 12699-12705 (2015).
10. J. Zirzlmeier, D. Lehnherr, P. B. Coto, E. T. Chernick, R. Casillas, B. S. Basel, M. Thoss, R. R. Tykwinski, D. M. Guldi, Singlet fission in pentacene dimers. *Proc. Natl. Acad. Sci. U. S. A.* **112**, 5325-5330 (2015).
11. A. A. Bakulin, S. E. Morgan, T. B. Kehoe, M. W. Wilson, A. W. Chin, D. Zigmantas, D. Egorova, A. Rao, Real-time observation of multiexcitonic states in ultrafast singlet fission using coherent 2D electronic spectroscopy. *Nat. Chem.* **8**, 16-23 (2016).
12. K. Miyata, F. S. Conrad-Burton, F. L. Geyer, X. Y. Zhu, Triplet Pair States in Singlet Fission. *Chem. Rev.* **119**, 4261-4292 (2019).
13. M. J. Y. Tayebjee, S. N. Sanders, E. Kumarasamy, L. M. Campos, M. Y. Sfeir, D. R. McCamey, Quintet multiexciton dynamics in singlet fission. *Nat. Phys.* **13**, 182-188 (2016).
14. L. R. Weiss, S. L. Bayliss, F. Kraffert, K. J. Thorley, J. E. Anthony, R. Bittl, R. H. Friend, A. Rao, N. C. Greenham, J. Behrends, Strongly exchange-coupled triplet pairs in an organic semiconductor. *Nat. Phys.* **13**, 176-181 (2016).
15. B. S. Basel, J. Zirzlmeier, C. Hetzer, B. T. Phelan, M. D. Krzyaniak, S. R. Reddy, P. B. Coto, N. E. Horwitz, R. M. Young, F. J. White, F. Hampel, T. Clark, M. Thoss, R. R. Tykwinski, M. R. Wasielewski, D. M. Guldi, Unified model for singlet fission within a non-conjugated covalent pentacene dimer. *Nat. Commun.* **8**, 15171 (2017).

16. Y. Kobori, M. Fuki, S. Nakamura, T. Hasobe, Geometries and Terahertz Motions Driving Quintet Multiexcitons and Ultimate Triplet-Triplet Dissociations via the Intramolecular Singlet Fissions. *J. Phys. Chem. B* **124**, 9411-9419 (2020).
17. S. L. Bayliss, L. R. Weiss, F. Kraffert, D. B. Granger, J. E. Anthony, J. Behrends, R. Bittl, Probing the Wave Function and Dynamics of the Quintet Multiexciton State with Coherent Control in a Singlet Fission Material. *Phys. Rev. X* **10**, 021070 (2020).
18. R. M. Jacobberger, Y. Qiu, M. L. Williams, M. D. Krzyaniak, M. R. Wasielewski, Using Molecular Design to Enhance the Coherence Time of Quintet Multiexcitons Generated by Singlet Fission in Single Crystals. *J. Am. Chem. Soc.* **144**, 2276-2283 (2022).
19. D. A. Hall, D. C. Maus, G. J. Gerfen, S. J. Inati, L. R. Becerra, F. W. Dahlquist, R. G. Griffin, Polarization-Enhanced NMR Spectroscopy of Biomolecules in Frozen Solution. *Science* **279**, 930-932 (1997).
20. J. H. Ardenkjær-Larsen, B. Fridlund, A. Gram, G. Hansson, L. Hansson, M. H. Lerche, R. Servin, M. Thaning, K. Golman, Increase in signal-to-noise ratio of >10,000 times in liquid-state NMR. *Proc. Natl. Acad. Sci. U. S. A.* **100**, 10158-10163 (2003).
21. S. E. Day, M. I. Kettunen, F. A. Gallagher, D. E. Hu, M. Lerche, J. Wolber, K. Golman, J. H. Ardenkjaer-Larsen, K. M. Brindle, Detecting tumor response to treatment using hyperpolarized 13C magnetic resonance imaging and spectroscopy. *Nat. Med.* **13**, 1382-1387 (2007).
22. A. J. Rossini, A. Zagdoun, M. Lelli, A. Lesage, C. Copéret, L. Emsley, Dynamic Nuclear Polarization Surface Enhanced NMR Spectroscopy. *Acc. Chem. Res.* **46**, 1942-1951 (2013).
23. J. M. Franck, A. Pavlova, J. A. Scott, S. Han, Quantitative cw Overhauser effect dynamic nuclear polarization for the analysis of local water dynamics. *Prog. Nucl. Magn. Reson. Spectrosc.* **74**, 33-56 (2013).
24. H. Nonaka, R. Hata, T. Doura, T. Nishihara, K. Kumagai, M. Akakabe, M. Tsuda, K. Ichikawa, S. Sando, A platform for designing hyperpolarized magnetic resonance chemical probes. *Nat. Commun.* **4**, 2411 (2013).
25. A. Ajoy, K. Liu, R. Nazaryan, X. Lv, P. R. Zangara, B. Safvati, G. Wang, D.Arnold, G. Li, A. Lin, P. Raghavan, E.Druga, S. Dhomkar, D. Pagliero, J. A. Reimer, D. Suter, C. A. Meriles, A. Pines, Orientation-independent room temperature optical 13C hyperpolarization in powdered diamond. *Sci. Adv.* **4**, eaar5492 (2018).
26. Q. Stern, S. F. Cousin, F. Mentink-Vigier, A. C. Pinon, S. J. Elliott, O. Cala, S. Jannin, Direct observation of hyperpolarization breaking through the spin diffusion barrier. *Sci. Adv.* **7**, eabf5735 (2021).
27. S. J. Nelson, J. Kurhanewicz, D. B. Vigneron, P. E. Z. Larson, A. L. Harzstark, M. Ferrone, M. van Criekinge, J. W. Chang, R. Bok, I. Park, G. Reed, L. Carvajal, E. J. Small, P. Munster, V. K. Weinberg, J. H. Ardenkjær-Larsen, A. P. Chen, R. E. Hurd, L. Odegardstuen, F. J. Robb, J. Tropp, J. A. Murray, Metabolic Imaging of Patients with Prostate Cancer Using Hyperpolarized [1-13C]Pyruvate. *Sci. Transl. Med.* **5**, 198ra108 (2013).
28. A. Henstra, J. Schmidt, T.-S. Lin, W. T. Wenckebach, High dynamic nuclear polarization at room temperature. *Chem. Phys. Lett.* **165**, 6-10 (1990).
29. S. Bogatko, P. D. Haynes, J. Sathian, J. Wade, J.-S. Kim, K.-J. Tan, J. Breeze, E. Salvadori, A. Horsfield, M. Oxborrow, Molecular Design of a Room-Temperature Maser. *J. Phys. Chem. C* **120**, 8251-8260 (2016).
30. E. M. M. Del Valle, Cyclodextrins and their uses: a review. *Process Biochem.* **39**, 1033-1046 (2004).
31. F. Würthner, T. E. Kaiser, C. R. Saha-Möller, J-Aggregates: From Serendipitous Discovery to Supramolecular Engineering of Functional Dye Materials. *Angew. Chem., Int. Ed.* **50**, 3376-3410 (2011).

Acknowledgments

The computations were partially performed at the Research Center for Computational Science, Okazaki, Japan (Project: 21-IMS-C043, 22-IMS-C043).

Funding: This work was partly supported by the JST-PRESTO program on “Creation of Life Science Basis by Using Quantum Technology” (JPMJPR18GB), JSPS KAKENHI (JP17H06375, JP19H02537, JP19H05718, JP19K15508, JP20H05106, JP20H02713, JP20K21211, JP20H05676, and JP21J13049); The Shinnihon Foundation of Advanced Medical Treatment Research; the Innovation Inspired by Nature Program of Sekisui Chemical Co. Ltd.; the RIKEN-Kyushu University of Science and Technology Hub

Collaborative Research Program; the RIKEN Cluster for Science, Technology and Innovation Hub (RCSTI); and the RIKEN Pioneering Project “Dynamic Structural Biology”.

Author contributions: Yu. K. and N. Y. conceived and designed the project. Yu. K., Y. N., and S. F. prepared and characterized the samples. S. S. and G. W. performed the MD simulations. T. R., T. T., M. S., K. O., and K. M. carried out the TAS measurements. Yu. K. and A. Y. measured the ESR spectra. A. Y. and Ya. K. simulated the ESR spectra. Yu. K., T. H., and K. N. carried out the DNP measurements. K. T. and T. U. contributed to building the ESR and DNP setup. Yu. K., A. Y., K. N., K. M., and N. Y. wrote the manuscript with contributions from all authors.

Competing interests: All authors declare they have no competing interests.